Environmental Science Nano

ROYAL SOCIETY OF CHEMISTRY

PAPER

View Article Online
View Journal | View Issue

Cite this: *Environ. Sci.: Nano*, 2021, **8**, 2641

Sulfur-containing nitrogen-rich robust hierarchically porous organic polymer for adsorptive removal of mercury: experimental and theoretical insights†

Avik Chowdhury, ‡[a] Sabuj Kanti Das, ‡[a] Saptarsi Mondal, [bc] Santu Ruidas,[a] Debabrata Chakraborty,[a] Sauvik Chatterjee, [a] Manas K. Bhunia, [d] Debraj Chandra, [d] Michikazu Hara [e] and Asim Bhaumik *[a]

Received 18th May 2021,
Accepted 23rd July 2021

DOI: 10.1039/d1en00448d

rsc.li/es-nano

The development of an efficient and robust material for adsorptive removal of highly toxic metals like mercury from water resources is very challenging from the perspectives of hygiene and sustainable environment. Heteroatoms such as sulfur and nitrogen in this high surface area porous organic polymer is very promising for mercury remediation because it offers strong interactions between Hg(II) ions and S/N bound at the pore surface of the adsorbent. Thus, herein we developed a new secondary amine-linked, sulfur-containing and N-rich porous organic polymer, TTP-1, *via* polycondensation of a tetrapodal amine and thiophene-2-carbaldehyde. TTP-1 displayed a high BET surface area of 1034 $m^2\ g^{-1}$ with hierarchical porosity and exceptionally high uptakes of 3106 and 691 mg g^{-1} for inorganic Hg^{2+} and organic methylmercury (CH_3Hg^+), respectively. The high adsorption efficiency for mercury capture is also supported from the strong noncovalent interaction of the ligand S and N lone pairs with Hg^{2+}, as revealed from the *ab initio* quantum chemical calculation and AIM analysis. Cost-effective, eco-friendly and scaleable synthesis of porous organic polymer with hierarchical porosity reported herein may contribute to the design of a benchmark adsorbent for the remediation of mercury (Hg(II)/CH_3Hg^+) and may significantly aid in industrial and environmental cleanup.

Environmental significance

Mercury poisoning is a serious environmental issue as it can affect the human body *via* contamination from air, water or soil. Adsorptive removal of mercury is the most desirable technology to combat this problem. Sulfur- and nitrogen rich high surface area porous organic polymers are very demanding for the adsorptive removal of mercury as high surface area enhances the Hg(II) adsorption capacity and these heteroelements present at the pore surface of the material offer strong interactions with Hg(II) ions. Herein, a secondary amine-linked, S-containing porous organic polymer, TTP-1 has been developed through the Schiff base polycondensation of a tetramine and a monoaldehyde. TTP-1 possess very high specific surface area together with hierarchical porosity and it showed exceptionally high uptakes for Hg^{2+} (3106 mg g^{-1}) and organic methylmercury (691 mg g^{-1}). *Ab initio* quantum chemical calculation and AIM analysis supported these high Hg uptakes. This work will provide highly advantageous blueprint for designing an efficient and cost-effective adsorbent for the removal of mercury from contaminated water sources.

Introduction

Technology-driven growth of our society is in urgent need of a remedy from heavy metal contamination and pollution,[1] which is a matter of great concern. The toxicity and non-biodegradability of heavy metals such as Hg(II), Cd(II), and Pb(II) intensify the issue.[2,3] Mercury is known to be naturally

[a] *School of Materials Sciences, Indian Association for the Cultivation of Science, 2A & 2B Raja S. C. Mullick Road, Jadavpur, Kolkata 700032, India. E-mail: msab@iacs.res.in*
[b] *Center for Molecular Spectroscopy and Dynamics, Institute of Basic Science (IBS), Seoul 02841, Republic of Korea*
[c] *Department of Chemistry, Korea University, Seoul 02841, Republic of Korea*
[d] *World Research Hub Initiative (WRHI), Institute of Innovative Research, Tokyo Institute of Technology, Midori-ku, Yokohama 226-8503, Japan*
[e] *Laboratory for Materials and Structures, Institute of Innovative Research, Tokyo Institute of Technology, Midori-ku, Yokohama 226-8503, Japan*

† Electronic supplementary information (ESI) available: Methodology, ^1H and ^{13}C NMR, powder XRD, FESEM images, TGA and solid UV-vis spectra. See DOI: 10.1039/d1en00448d

‡ These authors contributed equally.

occurring, but anthropogenic activities such as industrial emission, mining and huge irrigation of ground water have also contributed significantly to the accumulation of mercury in our biosphere.[4] The presence of mercury in several forms[5] such as metallic (Hg), organic (RHg^{+}) and inorganic (Hg^{2+}) compounds could affect our immune, nervous and digestive systems upon consumption through food or by inhalation, which causes adverse health issues such as impaired cognitive functions, kidney disorders, neurological problems and several other disabilities.[6] According to the report of the United Nations Environment Programme (UNEP 2018),[7] there is approximately 2000 tons of mercury emission taking place globally per year. Moreover, as per the guidelines of the World Health Organization (WHO), drinking water having mercury above 2 ppb level could be detrimental to mankind. Therefore, developing efficient strategies for the complete removal of mercury from polluted water to supply safe drinking water became a great challenge for researchers and environmentalists. There are some well-established methods such as chemical treatment,[8] ion exchange,[9] co-precipitation,[10] adsorption,[11] and complexation[12] already in practice. The adsorption-based Hg-removal strategy is found to be most feasible, durable and cost-effective[13] among these.

In recent times, porous nanomaterials are considered as an interesting class of materials because of their huge potential in various fields such as gas sorption,[14] catalysis,[15] and several energy harvesting applications[16] owing to their high BET surface area, tunable pore size and strong host–guest interactions. By virtue of these outstanding properties, these materials are extremely useful as potential adsorbents.[17] Several members of this special family of materials such as covalent organic frameworks (COFs),[18,19] porous organic polymers (POPs),[20] porous metal oxides,[21] metal organic frameworks (MOFs),[22–24] periodic mesoporous organosilicas (PMOs),[25] zeolites,[26] thiol-functionalized silicas,[27] and modified graphene oxide sheets have displayed high efficiency for the removal of toxic metals by virtue of their unique properties like scope of hetero atom introduction, structural integrity towards adsorption and recycling. Some of these are explored as benchmark materials for being robust adsorbents towards toxic metals.[28,29]

Therefore, keeping all these in mind herein, we synthesized a robust porous organic polymer (TTP-1) through one-pot poly-condensation[30] between a tetrapodal amine 6,6′-(1,4-phenylene)bis-(1,3,5-triazine-2,4-diamine) and thiophene-2-carbaldehyde. TTP-1 displays high BET surface area and possesses a large amount of heteroatoms such as nitrogen and sulfur that furnish an enormous number of chelating sites at the pore surface, and this has been successfully utilized for the adsorptive removal of aqueous and organic Hg (organic and inorganic). Hg(II) uptake displayed by TTP-1 is one of the leading mercury uptake amounts reported till date. The *ab initio* quantum mechanical calculation as well as AIM analysis was conducted, which further suggested the interaction between the N and S-sites of TTP-1 with mercury.

Experimental

Materials

All the chemicals were purchased and used without further purification. Thiophene-2-carboxaldehyde, 1,4-dicyanobenzene, 2-methoxyethanol and dicyandiamide were purchased from Sigma-Aldrich. Dimethyl sulphoxide (DMSO) and KOH were purchased from Merck, India. Methanol and other organic solvents were purchased from Finar Chemicals.

Characterization

An Anton Paar Monowave 300 microwave synthesis reactor were used for the synthesis of tetradentate amine monomers. The bonding connectivity on the material was investigated by recording FT-IR spectra using a Perkin Elmer Spectrum 100 spectrophotometer. Different carbon and proton environments of monomers were analysed by recording ^{1}H and ^{13}C NMR spectra in deuterated solvents using a Bruker Advance II NMR spectrometer. The presence of carbon environment of the insoluble polymeric material was investigated by ^{13}C CP MAS NMR spectroscopy at 8 kHz magic angle spinning frequency using a 4 nm MAS probe. The crystalline or amorphous phase of polymeric materials was investigated by analysing powder X-ray diffraction data recorded using a Bruker D8 Advance X-ray diffractometer, where Cu K_{α} (λ = 0.1541 nm) acts as a source of X-ray. Morphological characteristics of the as-synthesized materials were investigated from the HR TEM images acquired using a JEOL JEM 2010 electron microscope at an accelerating voltage of 200 kV. The elemental mapping of the material after Hg uptake was carried out by analysing FE-SEM analysis with JEOL JEM 6700 field emission scanning electron microscope. The porosity and specific surface area of TTP-1 were investigated by measuring the Brunauer–Emmett–Teller surface area with N_2 sorption at 77 K using a Quantachrome Autosorb iQ. Thermogravimetric analysis was carried out using a Perkin Elmer TA-SDTQ-600 thermogravimetric analyser (TGA) at a scanning rate of 10 °C min^{-1} in air. Metal ligand bonding is confirmed by solid-state UV-vis spectrum analysis using a Shimadzu UV-2401PC spectrophotometer. The elemental analysis (C, N, H and S) was carried out using a Perkin Elmer 2400 series II elemental analyser. The concentration of Hg was analysed by inductively coupled plasma optical emission spectroscopy (ICP-OES) using a Perkin Elmer Optima 2100 DV optical emission spectrometer. X-ray photoelectron spectroscopy was performed with the post mercury adsorbed TTP-1 using a Shimadzu ESCA-3400HSE (Mg Kα operated at 10 kV and 25 mA).

Synthesis of 6,6′-(1,4-phenylene)bis(1,3,5-triazine-2,4-diamine)

Amine monomer 6,6′-(1,4-phenylene)bis(1,3,5-triazine-2,4-diamine) was synthesized following the previously reported procedure[31] *via* one-pot synthetic strategy using a microwave reactor, where 1,4-dicyanobenzene (320 mg 2.5 mmol) and

dicyandiamide (420 mg, 5 mmol) were taken in G-30 vial. This is followed by the addition of 50 mg KOH in 10 ml 2-methoxyethanol solvent, after which the vial was put in a microwave reactor and allowed to react at 195 °C for 10 min (ESI,† Scheme S1). After the completion of the reaction, the whole reaction mixture was poured into hot water followed by filtration and washing with excess hot water. The synthesis was confirmed by recording the ^{1}H and ^{13}C NMR spectra (ESI,† Fig. S1 and S2).

Synthesis of TTP-1

The porous polymer TTP-1 was prepared *via* a simple Schiff base polycondensation reaction.[32] In a typical reaction, thiophene-2-carboxaldehyde and tetramine monomer [6,6′-(1,4-phenylene)bis(1,3,5-triazine-2,4-diamine)] were taken in a dry round-bottomed flask with 2 : 1 molar ratio, and then 20 ml of DMSO was added to it and the whole mixture was refluxed at 150 °C for 2 days (Scheme 1). After that, the mixture was cooled to room temperature and filtered off the precipitate followed by washing with DMSO followed by distilled water to afford a yellowish powder. Then, the product was washed successively with plenty of water, methanol, THF and acetone to remove DMSO and organic impurities. The final material was dried in an oven at 120 °C overnight and then characterized by ^{13}C CP MAS NMR, FT-IR, HR-TEM, powder XRD and N_2 sorption analyses.

Mercury uptake study

Mercury uptake over TTP-1 material was investigated by studying the mercury capture capacity from 30 ml of Hg(II) aqueous solutions with different concentrations using 25 mg of TTP-1 for 12 h. The uptake amounts are measured from the ICP-OES analysis of the solutions after filtering the adsorbent from the adsorbent–solute mixture. To study the kinetics of mercury, we used 2 ppm aqueous solution of Hg^{2+} by taking mercuric acetate [$Hg(OAc)_2$] as a Hg^{2+} precursor. The investigation was carried out using 20 mg, 25 mg and 40 mg of TTP-1 for 30 ml solutions. Out of these, 25 mg material exhibits significantly high mercury uptake. Thus, mercury uptake was studied with 30 ml of 2 ppm stock solutions using 25 mg material and the amount of mercury removed by TTP-1 was analysed by measuring the Hg^{2+} concentration of the aliquots taken at different time intervals. The efficiency of Hg uptake was calculated using eqn (1):

$$R = \frac{C_0 - C_t}{C_0} \times 100\% \quad (1)$$

where R is the removal efficiency, 'C_0' stands for the initial concentration of the stock solution and 'C_t' is the concentration after t-th time (in minutes).

Recyclability tests were carried out by washing the Hg-adsorbed TTP-1 with 2 N of HCl, followed by centrifugation and drying under high vacuum. Then, the uptake experiments were carried out up to 5 consecutive cycles. Considering the tremendous toxicity of organic mercury, we also studied the uptake of organic mercury using 25 ml 200 ppb and 500 ppb solution of methylmercury(II) iodide (CH_3-HgI) in methanol. The uptake capacities were studied using 25 mg of material for 25 ml of each solutions of methylmercury.

Results and discussion

We have synthesized a sulfur-containing nitrogen-rich aminal linked porous organic polymer, TTP-1, *via* an extended polycondensation reaction. The final as-synthesized material was found to be insoluble in all the common organic solvents confirming the formation of the extended polymeric network. In the following section, we summarize several spectroscopic and microscopic characterizations of TTP-1.

Spectroscopic characterization

FT-IR spectroscopic analysis was carried out to investigate the bonding connectivity in TTF-1 (Fig. 1). The complete attenuation of aldehydic stretching frequency at 1665 cm^{-1} and the appearance of a strong broad signal at 3380 cm^{-1} in TTP-1 indicate the formation of aminal (–NH–) linkage.[33]

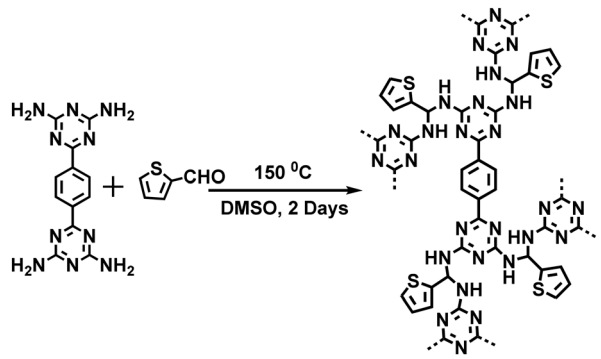

Scheme 1 Synthesis of TTP-1 from tetrapodal amine and aldehyde.

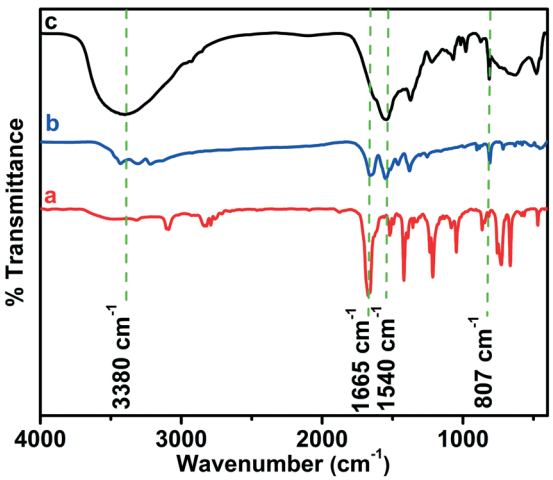

Fig. 1 FT-IR spectra of thiophene2-carboxaldehyde (a), tetramine ligand (b) and TTP-1 (c).

However, the presence of vibration bands at 1546 cm^{-1} and 807 cm^{-1} in the tetramine monomer as well as TTF-1 indicates the successful incorporation[34] of the triazine moiety in the polymeric network.

The ^{13}C CP MAS NMR spectra of TTP-1 displayed peaks at 166 and 173 ppm (Fig. 2) corresponding to the presence of triazine carbons (marked as d and e).[19] The carbon atoms of the thiophene ring adjacent to the S atom and aromatic C atoms adjacent to the triazine ring (marked as c) give a signal at 140 ppm. The broad peak observed at 127 ppm could be attributed to the sp^2 hybridized aromatic carbons (marked as b) of thiophene and benzene moieties. The broadened peak at 54 ppm could be attributed to the presence of sp^3 hybridized aminal linked carbon atom (marked as a).

Morphological analysis

High-resolution transmission electron microscopic (HRTEM) and field emission scanning electron microscopic (FESEM) images of TTP-1 are analyzed to understand the morphology, porosity and nanostructure. Spherical morphology with an average particle diameter of 15–20 nm together with the random void space in nanoscale is clearly seen in these HRTEM images (Fig. 3). Hg uptake over TTP-1 has been further investigated through elemental mapping in the FESEM analysis after Hg(II) adsorption. The elemental analysis result shown in Fig. 3V and VI suggests that higher S concentrations are responsible for higher Hg uptake due to the presence of preferable soft–soft acid–base interactions. The FESEM images of the Hg-adsorbed TTP-1 material after five adsorption cycles (ESI,† Fig. S3) were also collected, which confirmed the retention of spherical morphology in the presence of mercury.

Surface area and porosity analysis

The porosity and surface area of the as-synthesized POP material were analysed through a N_2 adsorption–desorption isotherm at 77 K (Fig. 4). This isotherm revealed the presence of a mixture of both types I and IV.[35] The steep rise of isotherm at low pressures could be attributed to the presence of micropores. The existence of inter-particle porosity in the material is evidenced from the sharp rise of the isotherm at high P/P_0. The hysteresis of H4 type that appeared at high P/P_0 could be attributed to the presence of interparticle void space.[20] The Brunauer–Emmett–Teller surface area (S_{BET}) was 1034 $m^2\ g^{-1}$ along with a total pore volume of 1.636 cc g^{-1}. The corresponding pore size distribution (PSD, inset of Fig. 4) estimated by the NLDFT method again corroborates the coexistence of both micropores and mesopores in the material. High surface area and the presence of hierarchical porosity (micropores and mesopores) together with S- and N-rich adsorption sites make TTP-1 a potential candidate for Hg(II) removal.

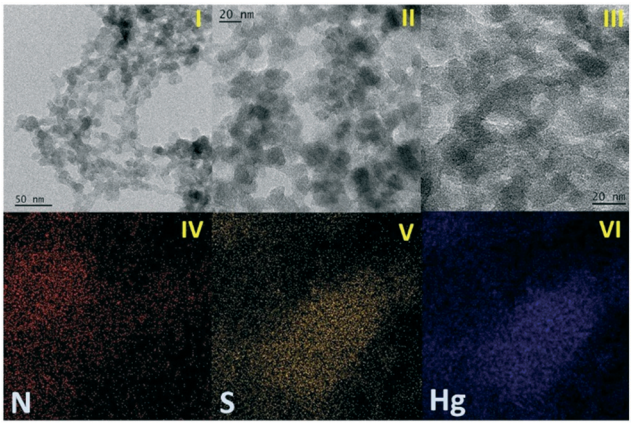

Fig. 3 Transmission electron microscopic images of TTP-1 (I–III) and SEM image showing the elemental mapping after Hg uptake (IV–VI).

Thermal stability, powder X-ray diffraction, UV-vis, XPS and elemental analysis

Thermal stability of the TTP-1 adsorbent was estimated from the thermogravimetric analysis (ESI,† Fig. S4a) under air flow.

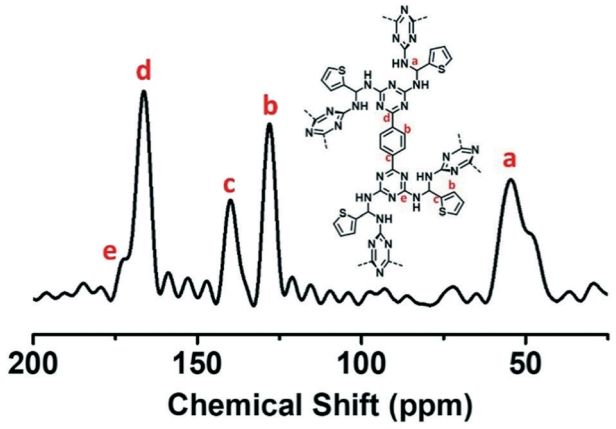

Fig. 2 ^{13}C CP MAS NMR spectrum of TTP-1. (a)–(e) Defines different carbon environments.

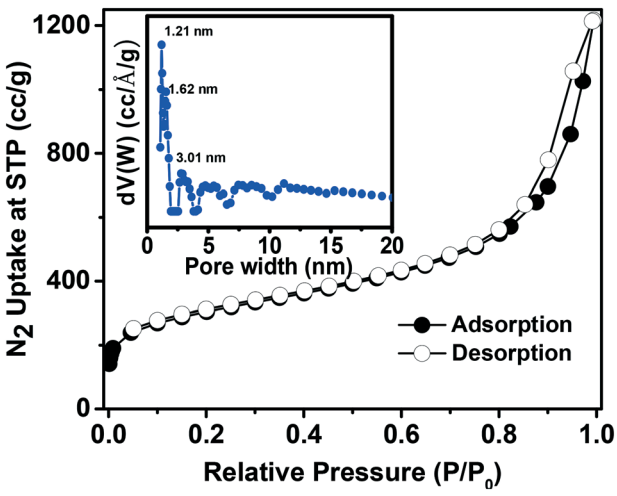

Fig. 4 N_2 adsorption/desorption isotherm of TTP-1 at 77 K. PSD plot is shown in the inset.

Here a weight loss of *ca.* 7 wt% was observed up to 74 °C, which could be attributed to the evaporation of surface adsorbed water molecules. Again on further increase in temperature, no significant weight loss was observed, which indicates that the material is thermally stable till 320 °C. Finally, in the temperature range of 320–580 °C, a rapid weight loss of *ca.* 70 wt% was observed, which suggested the collapse of a polymer network. Powder X-ray diffraction pattern of TTP-1 is shown in Fig. S4b (ESI†), which showed a broad hump at 2θ = 12 to 35°, suggesting mostly amorphous nature of the polymeric network.[30] Furthermore, the XRD analysis was carried out before (ESI,† Fig. S3b) and after the adsorption cycles (ESI,† Fig. S5), clearly indicating the unaffected polymeric network upon mercury capture.

Solid-state UV-vis spectroscopic analysis has been carried out for the as-synthesized and Hg-loaded materials (ESI,† Fig. S6). A drop in intensity along with red-shifted UV-vis spectra of the metal-loaded TTP-1 material confirmed that the Hg uptake has taken place.[36,37] Further to gain more insight about the presence of mercury and bonding interaction with TTP-1, X-ray photo electron spectroscopy (XPS) was conducted with the post adsorbed TTP-1. The presence of strong signals at 101.8 eV and 105.8 eV (Fig. 5a) could be attributed to $Hg4f_{7/2}$ and $Hg4f_{5/2}$, respectively.[38] This Hg 4f spectrum reveals the presence of mercury. In addition to this, the appearance of strong peaks at higher binding energies of 164.5 eV for $S2p_{3/2}$ and 165.9 eV for $S2p_{1/2}$ (Fig. 5b)[11] suggested the presence of sulphur in the material that interacts with mercury. The bonding interactions were also in agreement with the quantum mechanical study results. Elemental analysis has been carried out to investigate the percentage of elements present in the polymer network, where we found the percentage of C, H, N and S as 52.1, 4.3, 31.3 and 12.3% respectively. Higher density of hetero atoms (N and S) contained in the TTP-1 POP lead us to perform the mercury uptake application as different types of nonbonding interaction between the host framework and guest metal ions (Hg ions) could be possible.

Mercury adsorption

The TTP-1 material contains high percentages of N and S on the surface of this material that are able to act as soft binding sites. Hence, it is expected to have a strong affinity towards adsorption of soft metal ions such as mercury, lead, and cadmium. On allowing the material for long-time mercury capture, TTP-1 shows an excellent uptake capability of Hg^{2+}. The highest uptake of the toxic mercury(II) ion by the material was found to be 3106 mg g^{-1} of Hg^{2+}, observed from ICP-OES analysis data when the material is allowed to interact with a series of aqueous solution of different Hg^{2+} concentrations. The Langmuir isotherm (Fig. 6a) plot was conducted over different concentrations of Hg(II), which confirms the aforesaid conclusion ($R^2 > 0.99$). To the best of our knowledge, this is the second highest Hg(II) uptake by any type of adsorbent reported till date after imine-based thiol-functionalized COF TPB-DMTP-COF-SH.[39] Soft–soft acid–base interactions ($S\cdots Hg^{+/++}$), presence of several chelating donor sites and free rotation of the thiophene moiety in TTP-1 offer a large scope in the host–guest binding probabilities. All these features collectively help TTP-1 to show high Hg(II) uptake.

Considering the tremendous toxicity of organic mercury, the methylmercury uptake studies were carried out using 200 ppb and 500 ppb solutions of methyl mercury (CH_3-Hg^+) in methanol. The material exhibited removal efficiencies of 98.62% and 98.30% within 30 minutes from the 200 and 500 ppm CH_3Hg^+ solutions, respectively. The highest uptake of CH_3Hg^+ was found to be 690 mg g^{-1}, which is quite high considering the state-of-the-art organic mercury removing adsorbents reported till date. The value is found to be more than 5 and 15 times higher than that of previously reported GOS[40] and SGO/Fe-Mn,[41] systems. In Table 1, we have provided a comparison table for the benchmark adsorbents reported in the literature for adsorptive removal of mercury.

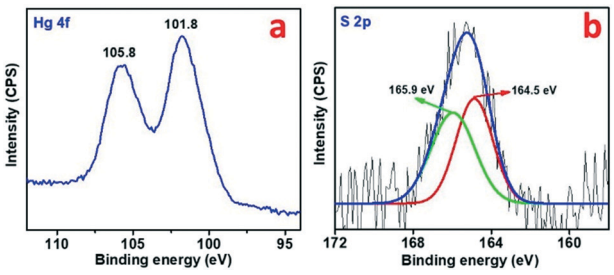

Fig. 5 XPS spectrum of TTP-1, after mercury adsorption (a) Hg 4f and (b) S 2p.

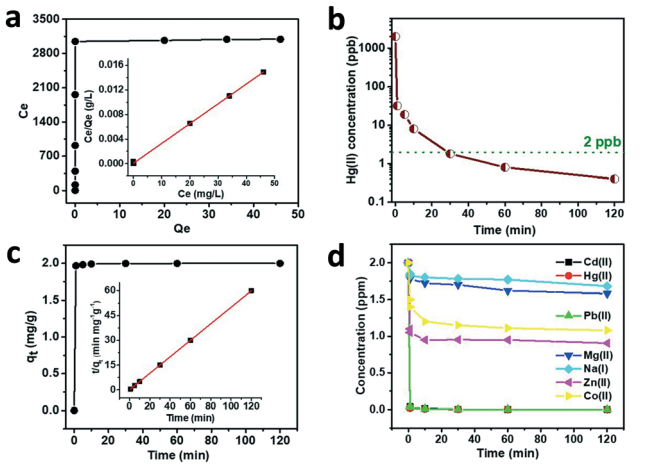

Fig. 6 (a) Hg uptake for long contact time (12 h) fit of the data with the Langmuir model by linear regression shown in inset. (b) Adsorption analysis using 2 ppm Hg^{2+} aqueous medium at different time intervals. (c) Hg(II) adsorption *versus* contact time in the aqueous solution for 2 ppm. Pseudo-second-order kinetic plot for the adsorption at a Hg(II) concentration of 2 ppm is shown in the inset. (d) Activity of the material towards other metal and heavy metal ions.

Table 1 Comparison of TTP-1 for mercury uptake capacities *vis-à-vis* benchmark adsorbents

Entry	Material	Hg uptake (mg g^{-1})		Ref.
		Hg(II)	CH_3Hg^+	
1.	DMTZ-PMO	2081	281	25
2.	POP-SH	1216	—	28
3.	PAF-1-SH	1350	—	29
4.	GOS	449.6	127	40
5.	SGO/Fe–Mn-am		48	41
6.	PANI/RGO	1000	—	42
7.	W-DR-N-MoS_2	2506	—	43
8.	$H_{1.45}Na_{0.45}InS_{2.45}$	2173	—	44
9.	MSWCNT–CoS	1666	—	45
10.	Starch-FeS	1998	—	46
11.	**TTP-1**	**3106**	**691**	**This work**

Hg^{2+} uptake kinetics

The kinetics of Hg uptake was conducted by measuring the Hg^{2+} concentration *via* ICP-OES analysis of the aliquots taken from the 2 ppm solution at different time scales. The data clearly show that the concentration of Hg(II) in the solution drops to 1.8 ppb within 30 minutes (Fig. 6b). This result is quite promising for reasonably fast mercury removal. The uptake data were found to be fitted well on the Ho and McKay[47] model of pseudo-second-order kinetics. The rate constant and equilibrium uptake were calculated using eqn (2):

$$\frac{t}{q_t} = \frac{1}{k_2 q_e^{\,2}} + \frac{t}{q_e} \quad (2)$$

where q_t and q_e imply Hg uptake at t-th time and at equilibrium respectively; k_2 signifies the second-order rate constant. The rate constant and equilibrium uptake were calculated from the slope and intercept (inset, Fig. 6c) respectively. The rate constant was found to be 15.56 g mg g^{-1} min^{-1} along with a correlation coefficient (R-square) of 0.998, which is quite a good value, indicating well define fitting in Ho MaKay kinetics. Though the value of k_2 is not very high compared to our previously reported SCTN-1 (ref. 20) having k_2 55.5 g mg^{-1} min^{-1} but it is quite comparable to several benchmark Hg(II) adsorbents reported in the literature. For example, TAPB-BMTTPA-COF[48] produces a k_2 value of 6.31 g mg^{-1} min^{-1}, showing almost two-fold higher values than that of the thiol-functionalized PAF-1-SH.[30]

The distribution coefficient for Hg uptake can also be calculated from eqn (3):

$$K_d = \frac{C_0 - C_e}{C_e} \times \frac{V}{m} \quad (3)$$

where K_d defines the distribution coefficient, C_0 and C_e implies the initial concentration and equilibrium concentrations respectively, V is the volume of the solution used for the study, and m is the amount of used material expressed in grams. The K_d value for TTP-1 was found to be 1.404×10^6 ml g, and the distribution coefficient value further reflects its high adsorptive separation ability. Fig. 6d depicts the selectivity of TTP-1 for different metal ions. The uptake experiments were conducted over 2 ppm solutions of Na^+, Mg^{2+}, Zn^{2+}, and Co^{2+} along with the heavy metal solution of Cd^{2+}, Hg^{2+} and Pb^{2+}. The plot clearly reveals the selectivity of TTP-1 towards soft metal ions such as cadmium, mercury and lead, while low uptake towards hard metals ions such as sodium and magnesium along with moderate uptake upon borderline metal ions such as zinc and cobalt. Furthermore, we carried out selectivity in the adsorption by taking higher concentrations of other ions. The tests were carried out using a solution containing 100 ppm of Na^+, Mg^{2+}, Zn^{2+}, and Co^{2+} along with 1 ppm of Cd^{2+}, Hg^{2+} and Pb^{2+}, and the results are listed in Table S1 (ESI†). This adsorption study suggested highly selective adsorption of heavy metal ions over the alkali/alkaline earth/transition metal ions by TTP-1 with a decreasing selectivity in the order of Hg(II) > Cd(II) > Pb(II).

Fig. 7 represents the recycling efficiency of TTP-1 for repetitive mercury uptakes from 2 ppm aqueous solutions. This recycling experiments were carried out over five consecutive adsorption cycles and as seen from Fig. 7 that TTP-1 has retained high efficiency for Hg(II) uptake in these consecutive adsorption cycles. This result suggested very promising future of TTP-1 for long-term mercury removal. Moreover, the retention of the powder XRD pattern of the recycled adsorbent clearly confirms (ESI,† Fig. S6) the structural integrity of TTP-1 in this prolonged aqueous treatments. The influence of pH on mercury capture was also investigated using 2 ppm Hg(II) solutions having various pH values (pH 2–10). In Fig. S7 (ESI†), we show the mercury removal efficiency of TTP-1 at different pH values. From this result, it is clear that the TTP-1 material is efficient for the Hg(II) removal for a wide range of pH values. Moreover, we determined out the Hg(II) uptake capacity from an real industrial wastewater sample collected from the effluent of nearby Durgapur thermal power station. The total Hg(II) content present in this wastewater sample was 2.74 ppm before treatment, and this was reduced to 1.9 ppb after treating with 25 mg of TTP-1 for 1 h. This result indicated excellent potential of our sulphur-containing N-rich porous

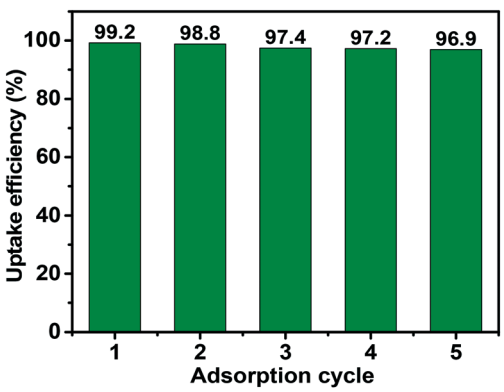

Fig. 7 Recyclability of TTP-1 towards Hg(II) uptake.

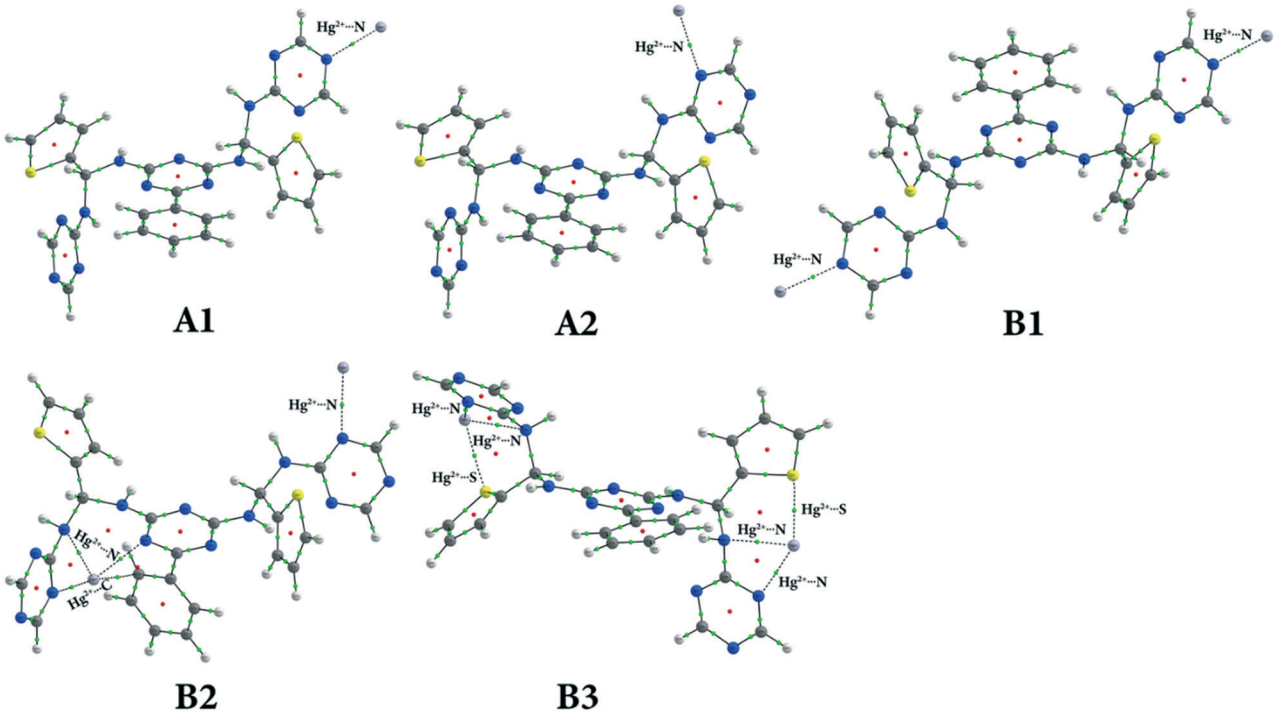

Fig. 8 Molecular density map of 1 : 1 complexes (A1–A2) and 1 : 2 complexes (B1–B3) between the model monomer and Hg^{2+} generated from the wavefunction calculated from of the optimized geometry at B3LYP density functional method using 6-31+G(d) basis set for C, H, N, and S and LanL2DZ basis set with effective core potential for Hg^{2+}. The green spheres indicate the bond critical point (BCP), and the red spheres represent the ring critical point (RCP). The spheres in white, grey, yellow, blue, and light grey represent H, C, S, N, and Hg atoms. The presence of very strong $Hg^{2+}\cdots N$ and $Hg^{2+}\cdots S$ interactions explain very high stabilization energy of the complexes.

TTP-1 material for Hg(II) capture from real wastewater samples.

To understand the underlying mechanism of how Hg^{2+} adsorbs into the porous polymer surface so well, mono- and di-mercuric complexes of various conformations of the repetitive unit of the material (ligand) with the Hg^{2+} ion was optimized using the B3LYP density functional, LanL2DZ basis set for Hg^{2+} with an effective core potential and 6-31+G(d) for all other atoms. We have obtained two mono-mercuric complexes (A1–A2) and three di-mercuric complexes (B1–B3) after geometry optimization. The molecular density map of all the complexes was generated at the same DFT level shown in Fig. 8, where the green sphere represents the bond critical point (BCP), and the red spheres represent the ring critical point (RCP).

The zero-point vibrational energy-corrected stabilization energy of all the complexes along with the bonding distances corresponding to different noncovalent interactions are tabulated in Table 2. The stabilization energies of mono-mercuric complexes such as A1 and A2 are 200.2 and 192.1 kcal per mole, which suggest their excellent stability. The stabilization energy of B1, B2, and B3 are 255.6, 235.8 and 225.1 kcal per mole respectively, which indicates their increased stability from the mono-mercuric complexes. Additionally, the most stable conformation obtained from (1 : 1) and (1 : 2) complexes between the model monomer and CH_3Hg^+ is shown in Fig. S8 of the ESI,† which reveals that the porous material could significantly adsorb CH_3Hg^+ as well. To understand the bonding nature of these mono- and di-mercuric complexes, the AIM analysis was performed to

Table 2 List of stabilization energy (ΔE_{Stab}, kcal per mole), electron density (ρ, a.u.), Laplacian of electron density ($\nabla^2\rho$, a.u.), and ellipticity (ε) at the BCPs of different noncovalent interactions in the mono- and di-mercuric complexes A1–A2 and B1–B3 calculated at B3LYP/6-31+G(d); LanL2DZ(Hg) level of theory

Complex	ΔE (kcal per mole)	Interaction	Distance (Å)	ρ	$\nabla^2\rho$	ε
	1 : 1 complex					
A1	200.2	$Hg^{2+}\cdots N$	2.68	0.031	0.096	0.07
A2	192.1	$Hg^{2+}\cdots N$	2.89	0.021	0.059	0.07
	1 : 2 complex					
B1	255.6	$Hg^{2+}\cdots N$	2.51	0.044	0.129	0.07
		$Hg^{2+}\cdots N$	2.49	0.046	0.165	0.07
B2	235.8	$Hg^{2+}\cdots N$	2.64	0.034	0.101	0.07
		$Hg^{2+}\cdots N$	2.47	0.047	0.163	0.07
		$Hg^{2+}\cdots N$	2.62	0.034	0.115	0.03
		$Hg^{2+}\cdots N$	2.37	0.057	0.186	0.06
		$Hg^{2+}\cdots C$	2.48	0.048	0.098	0.09
B3	225.1	$Hg^{2+}\cdots N$	2.36	0.043	0.136	0.02
		$Hg^{2+}\cdots N$	2.69	0.053	0.175	0.06
		$Hg^{2+}\cdots S$	2.69	0.044	0.096	0.03
		$Hg^{2+}\cdots N$	2.40	0.031	0.099	0.05
		$Hg^{2+}\cdots N$	2.54	0.058	0.193	0.06
		$Hg^{2+}\cdots S$	2.72	0.047	0.101	0.04

calculate the electron density (ρ), Laplacian of electron density ($\nabla^2\rho$), and ellipticity at different bond critical points (BCPs) along with the bonding distances. All the topological parameters corresponding to a particular interaction are tabulated in Table 2. Strong $Hg^{2+}\cdots N$ interaction can be observed in both A1 and A2 with bonding distances of 2.68 and 2.89 Å, respectively. The ρ and $\nabla^2\rho$ corresponding to $Hg^{2+}\cdots N$ interaction are 0.031 and 0.096 a.u. for A1 and 0.021 and 0.059 a.u. for A2. These higher topological parameters for A1 and A2 suggest a strong noncovalent interaction between Hg^{2+} and the N atom of the ligand in both these cases. The number of such strong noncovalent interactions increases in the di-mercuric complexes. The most stable conformation of the di-mercuric complexes B1 shows two $Hg^{2+}\cdots N$ interactions with reduced bonding distances of 2.51 and 2.49 Å compared to the mono-mercuric complexes with the respective ρ values of 0.044 and 0.046 a.u. and $\nabla^2\rho$ of 0.129 and 0.165 a.u. Similarly, B2 and B3 show multiple $Hg^{2+}\cdots N$ interactions along with $Hg^{2+}\cdots C$ (B2) and $Hg^{2+}\cdots S$ (B3) with higher topological parameters, which account for their excellent stability. The trend of the topological parameters corresponding to the various noncovalent interactions in these complexes shows that $Hg^{2+}\cdots N$ is a very strong interaction, whereas $Hg^{2+}\cdots S$ and $Hg^{2+}\cdots C$ are moderately strong noncovalent interactions.

The bond ellipticity (ε) values at the BCPs of $Hg^{2+}\cdots S/N/C$ interactions of all the complexes are tabulated in Table 2. The ellipticity measures the anisotropy of the electron density at a BCP. ε value close to zero for an interaction referring to the significant σ-bond character. The ε values for the $Hg^{2+}\cdots N$ and, $Hg^{2+}\cdots S$, and $Hg^{2+}\cdots C$ interactions for all the complexes are around 0.03 to 0.08, which are very low. This result indicates that these metal–surface interactions are very strong and have profound sigma bond characters.

Conclusions

A new hierarchically porous organic polymer, TTP-1, has been developed *via* a catalyst-free route involving polycondensation of a tetrapodal amine and thiophene-2-carbaldehyde. The porous polymer displayed exceptionally high specific surface area and high affinity towards mercury capture *via* soft–soft metal ligand interactions. The highest mercury(II) uptake was found to be 3106 mg g^{-1} within a period of 12 h with very high recyclability. Furthermore, this sulphur-containing and N-rich porous polymer shows an excellent activity towards the removal of extremely toxic methylmercury having the highest uptake amount of 691 mg g^{-1}. We have investigated the bonding nature of various noncovalent interactions between Hg^{2+} and the ligand sites present in the POP network using *ab initio* quantum chemical calculations and AIM analysis to understand the very high uptake capability and how Hg^{2+} adsorption by the material occurs. The ZPVE-corrected stabilization energy of the complex suggests that one ligand can efficiently bind at least two Hg^{2+}. The AIM analysis confirms that Hg^{2+} interacts with the N and S lone pair of the porous polymer *via* very strong noncovalent interactions. Therefore, the high Hg^{2+} adsorption by this porous organic polymer material could be attributed to the presence of strong to moderately stronger noncovalent interactions between Hg^{2+} and the ligand sites of the polymer surface. The high potentiality of TTP-1 towards the adsorptive removal of both organic and inorganic mercury can offer its huge environmental application and provide significant advancement for developing a sustainable adsorbent for the wastewater treatment.

Author contributions

AC, SKD and AB conceived the idea of this work. AC and SKD did detail physical characterizations. AC wrote the manuscript with the aid of all authors. SR, SC and DC helped data analysing and mercury uptake study. SM did computational calculations. MKB, DC and MH did the XPS analysis. The whole work has been done under the supervision of AB.

Conflicts of interest

There are no conflicts to declare.

Acknowledgements

AC and SR wish to thank CSIR, New Delhi for their senior research fellowship. SKD wishes to thank UGC, New Delhi and IACS for his senior research fellowship. DC and SC wish to thank DST-Inspire, New Delhi for their senior research fellowship. AB wishes to thank DST, New Delhi for funding through DST-SERB core research grant (Project no. CRG/2018/00230).

Notes and references

1 J. O. Nriagu, *Science*, 1996, **272**, 223–224.
2 M. McNutt, *Science*, 2013, **341**, 1430.
3 D. P. Krabbenhoft and E. M. Sunderland, *Science*, 2013, **341**, 1457–1458.
4 Q. Wang, D. Kim, D. D. Dionysiou, G. A. Sorial and D. Timberlake, *Environ. Pollut.*, 2004, **131**, 323–336.
5 M. E. Goodsite, J. M. C. Plane and H. Skov, *Environ. Sci. Technol.*, 2004, **38**, 1772–1776.
6 C. T. Driscoll, R. P. Mason, H. M. Chan, D. J. Jacob and N. Pirrone, *Environ. Sci. Technol.*, 2013, **47**, 4967–4983.
7 *Global Mercury Assessment 2018*, UNEP, UN Environment, 2019.
8 H. Shamsijazeyi and T. Kaghazchi, *J. Ind. Eng. Chem.*, 2010, **16**, 852–858.
9 J. M. Monteagudo and M. J. Ortiz, *J. Chem. Technol. Biotechnol.*, 2000, **75**, 767–772.
10 G. Guan, S.-Y. Zhang, Y. Cai, S. Liu, M. S. Bharathi, M. Low, Y. Yu, J. Xie, Y. Zheng, Y.-W. Zhang and M. Y. Han, *Chem. Commun.*, 2014, **50**, 5703–5705.
11 D. Zhang, L. Wang, H. Zeng, B. Rhimi and C. Wang, *Environ. Sci.: Nano*, 2020, **7**, 793–802.

12 J. B. Zambrano, S. Laborie, P. Viers, M. Rakib and G. Durand, *Desalination*, 2002, **144**, 201–206.
13 A. Modak, P. Bhanja, M. Selvaraj and A. Bhaumik, *Environ. Sci.: Nano*, 2020, **7**, 2887.
14 S. K. Das, P. Bhanja, S. K. Kundu, S. Mondal and A. Bhaumik, *ACS Appl. Mater. Interfaces*, 2018, **10**, 23813–23824.
15 Y. Zhang and S. N. Riduan, *Chem. Soc. Rev.*, 2012, **41**, 2083–2094.
16 Z. H. Xiang and D. P. Cao, *J. Mater. Chem. A*, 2013, **1**, 2691–2718.
17 Z. Wu and D. Zhao, *Chem. Commun.*, 2011, **47**, 3332–3338.
18 S.-Y. Ding, M. Dong, Y.-W. Wang, Y.-T. Chen, H.-Z. Wang, C.-Y. Su and W. Wang, *J. Am. Chem. Soc.*, 2016, **138**, 3031–3037.
19 Q. Sun, B. Aguila, J. Perman, L. D. Earl, C. W. Abney, Y. Cheng, H. Wei, N. Nguyen, L. Wojtas and S. Ma, *J. Am. Chem. Soc.*, 2017, **139**, 2786–2793.
20 S. Mondal, S. Chatterjee, S. Mondal and A. Bhaumik, *ACS Sustainable Chem. Eng.*, 2019, **7**, 7353–7361.
21 J.-S. Hu, L.-S. Zhong, W.-G. Song and L.-J. Wan, *Adv. Mater.*, 2008, **20**, 2977.
22 J. Cai, X. Mao and W.-G. Song, *Mater. Chem. Front.*, 2018, **2**, 1389–1396.
23 T. He, Y. Z. Zhang, X. J. Kong, J. Yu, X. L. Lv, Y. Wu, Z. J. Guo and J. R. Li, *ACS Appl. Mater. Interfaces*, 2018, **10**, 16650–16659.
24 T. Islamoglu, Z. Chen, M. C. Wasson, C. T. Buru, K. O. Kirlikovali, U. Afrin, M. R. Mian and O. K. Farha, *Chem. Rev.*, 2020, **120**, 8130–8160.
25 S. Das, S. Chatterjee, S. Mondal, A. Modak, B. K. Chandra, S. Das, G. D. Nessim, A. Majee and A. Bhaumik, *Chem. Commun.*, 2020, **56**, 3963–3966.
26 M. Yin, Z. Li, Z. Liu, X. Yang and J. Ren, *ACS Appl. Mater. Interfaces*, 2012, **4**, 431–437.
27 M. Kalantari, Z. Gu, Y. Cao, C. Lei and J. Zhang, *Environ. Sci.: Nano*, 2020, **7**, 851–860.
28 B. Aguila, Q. Sun, J. A. Perman, D. L. Earl, C. W. Abney, R. Elzein, R. Shlaf and S. Ma, *Adv. Mater.*, 2017, **29**, 1700665.
29 B. Li, Y. Zhang, D. Ma, Z. Shi and S. Ma, *Nat. Commun.*, 2014, **5**, 5537.
30 M. A. Sabri, M. H. A. Sayah, S. Sen, T. H. Ibrahim and Q. M. E. Kadri, *Sci. Rep.*, 2020, **10**, 15943.
31 S. K. Das, S. Mondal, S. Chatterjee and A. Bhaumik, *ChemCatChem*, 2018, **10**, 2488–2495.
32 M. G. Schwab, B. Fassbender, H. W. Spiess, A. Thomas, X. Feng and K. Müllen, *J. Am. Chem. Soc.*, 2009, **131**, 7216–7217.
33 S. K. Das, A. Chowdhury, D. Chakraborty, U. Kayal and A. Bhaumik, *Mol. Catal.*, 2020, **497**, 111198.
34 S. K. Kundu and A. Bhaumik, *RSC Adv.*, 2015, **5**, 32730–32739.
35 S. Mondal and N. Das, *J. Mater. Chem. A*, 2015, **3**, 23577–23586.
36 I. O. Jimenez, X. Lopez, J. Arbioi and V. Puntes, *ACS Nano*, 2012, **6**, 2253–2260.
37 J. Wang, R. Zhang, Y. Liu, Z. Wang, P. Wang, Z. Zheng, X. Qin, X. Zhang, Y. Dai and B. Huang, *Chem. Commun.*, 2018, **54**, 7195–7198.
38 Z. Yang, Y. Gu, B. Yuan, Y. Tian, J. Shang, D. C. W. Tsang, M. Liu, L. Gan, S. Mao and L. Li, *J. Hazard. Mater.*, 2021, **403**, 123702.
39 L. Meri-Bofi, S. Royuela, F. Zamora, M. L. Ruiz-Gonzalez, J. L. Segura, R. Munoz-Olivas and M. J. Mancheno, *J. Mater. Chem. A*, 2017, **5**, 17973–17981.
40 S. Xia, Y. Huang, J. Tang and L. Wang, *Environ. Sci. Pollut. Res.*, 2019, **26**, 8709–8720.
41 Y. Huang, J. Tang, L. Gai, Y. Gong, H. Guan, R. He and H. Lyu, *Chem. Eng. J.*, 2017, **319**, 229–239.
42 R. Li, L. Liu and F. Yang, *Chem. Eng. J.*, 2013, **229**, 460–468.
43 K. Ai, C. Ruan, M. Shen and L. Lu, *Adv. Funct. Mater.*, 2016, **26**, 5542–5549.
44 C. W. Abney, J. C. Gilhula, K. Lu and W. Lin, *Adv. Mater.*, 2014, **26**, 7993.
45 H. Alijani and Z. Shariatinia, *Chem. Eng. Res. Des.*, 2018, **129**, 132–149.
46 Y. Sun, Y. Liu, Z. Lou, K. Yang, D. Lv, J. Zhou, S. A. Baig and X. Xu, *Chem. Eng. J.*, 2018, **344**, 616–624.
47 Y. S. Ho and G. McKay, *Process Biochem.*, 1999, **34**, 451–465.
48 N. Huang, L. Zhai, H. Xu and D. Jiang, *J. Am. Chem. Soc.*, 2017, **139**, 2428–2434.